2014

Structural and electronic origin of the magnetic structures in hexagonal LuFeO3

Hongwei Wang
Temple University

Igor V. Solovyev
National Institute of Materials Science

Wenbin Wang
Fudan University

Xiao Wang
Bryn Mawr College

Philip J. Ryan
Argonne National Laboratory

See next page for additional authors

Structural and electronic origin of the magnetic structures in hexagonal $LuFeO_3$

Hongwei Wang,[1,2] Igor V. Solovyev,[3] Wenbin Wang,[4] Xiao Wang,[5] Philip J. Ryan,[6] David J. Keavney,[6] Jong-Woo Kim,[6] Thomas Z. Ward,[7] Leyi Zhu,[8] Jian Shen,[4] X. M. Cheng,[5] Lixin He,[2] Xiaoshan Xu,[5,7,9,*] and Xifan Wu[1,*]

[1]*Department of Physics, Temple University, Philadelphia, Pennsylvania 19122, USA*

[2]*Key Laboratory of Quantum Information, University of Science and Technology of China, Hefei, Anhui 230026, People's Republic of China*

[3]*Computational Materials Science Unit, National Institute for Materials Science, 1-2-1 Sengen, Tsukuba 305-0047, Japan*

[4]*Department of Physics, Fudan University, Shanghai 200433, People's Republic of China*

[5]*Department of Physics, Bryn Mawr College, Bryn Mawr, Pennsylvania 19010, USA*

[6]*Advanced Photon Source, Argonne National Laboratory, Argonne, Illinois 60439, USA*

[7]*Materials Science and Technology Division, Oak Ridge National Laboratory, Oak Ridge, Tennessee 37831, USA*

[8]*Materials Science Division, Argonne National Laboratory, Argonne, Illinois 60439, USA*

[9]*Department of Physics and Astronomy, University of Nebraska, Lincoln, Nebraska 68588, USA*

(Received 16 February 2014; revised manuscript received 7 July 2014; published 29 July 2014; corrected 15 August 2014)

Using combined theoretical and experimental approaches, we studied the structural and electronic origin of the magnetic structure in hexagonal $LuFeO_3$. Besides showing the strong exchange coupling that is consistent with the high magnetic ordering temperature, the previously observed spin reorientation transition is explained by the theoretically calculated magnetic phase diagram. The structural origin of this spin reorientation that is responsible for the appearance of spontaneous magnetization, is identified by theory and verified by x-ray diffraction and absorption experiments.

DOI: 10.1103/PhysRevB.90.014436 PACS number(s): 75.85.+t, 77.55.Nv

I. INTRODUCTION

While the ferroelectricity in materials is naturally connected to structural distortions that break the spatial inversion symmetry [1,2], the relation between spontaneous magnetization and structure is not obvious because no spatial symmetry is broken by ferromagnetism (FM). Nevertheless, magnetic orderings in a material are tied to the structure, and the ties are particularly important in multiferroic materials [3] in which structural distortions may mediate couplings between ferroelectricity and ferromagnetism or even generate ferroelectric ferromagnets, which are extremely rare [4].

The recently discovered room temperature multiferroic, i.e., hexagonal $LuFeO_3$ (hLFO) [5], provides a rare case of multiferroic material in which spontaneous electric and magnetic polarizations coexist. On one hand, ferroelectricity appears below $T_C = 1050$ K resulting from a $P6_3/mmc \rightarrow P6_3cm$ structure distortion, which can be decomposed in terms of three phonon modes [Fig. 1(a)] [5,6]. On the other hand, spin frustration in hLFO presents rich magnetic phases [7]. Intriguingly, below the Neél temperature $T_N = 440$ K, magnetic order in hLFO transits again from B_2 to A_2 [Fig. 1(b)] at $T_R = 130$ K [5] by a spin reorientation (SR), resulting in a weak ferromagnetism due to the Dzyaloshinskii-Moriya and single-ion anisotropy mechanism [8–12]. Similar to hexagonal $YMnO_3$, the K_3 phonon is believed to be the driving force that induces the instability of Γ_2^- that is responsible for the ferroelectricity [13–15]. However, the origin of the SR is still elusive. Since the SR is the direct cause of spontaneous magnetization, elucidating the origin may provide a way to effectively tune T_R, or even a novel route for realizing a coexistence of spontaneous electric and magnetic polarizations above room temperature [16–18].

Previous studies in hexagonal manganites (h-RMO, isomorphic to hLFO) indicate rich magnetic phases due to the SR that is strongly coupled to the crystal structure [3,19,20]. However, the multiple degrees of freedom involved (spin and orbital degrees of freedom of the electrons and the lattice) complicate the problem in h-RMO [21]. The complexity may be reduced in h-LFO, in which Fe^{3+} can be considered a spin-only ion with nearly spherical $3d^5$ electronic configuration. Therefore, a better understanding of the SR in hLFO is possible, particularly in terms of the phonon modes [Fig. 1(b)]; it may also be an important step in understanding the more complex SR in h-RMO [21], in which the single-ion anisotropy is expected to play a more important role.

To address the above issues, we perform combined theoretical and experimental studies of the exchange interactions and their couplings to the structural instabilities in hLFO. We apply an extended Kugel-Khomskii (KK) model for superexchange (SE) interactions [22] based on localized Wannier functions (LWFs) [23,24]. While the antiferromagnetic (AFM) exchange coupling is dominated by the intralayer superexchange, the model clearly shows that the singly occupied d_{z^2} orbital in hLFO greatly increases the exchange coupling compared with the empty d_{z^2} in $LuMnO_3$ (LMO). The interlayer exchange, although much weaker in magnitude, is key to the SR. Our first-principles calculations show that SR is strongly coupled to the K_1 phonon mode and only weakly dependent on K_3 mode. Our theory indicates that the atomic displacements of K_1 mode is responsible for the SR. This scenario is then confirmed by our x-ray diffraction and x-ray absorption experiments.

II. COMPUTATIONAL METHODS AND EXPERIMENTAL TECHNIQUES

Our extended KK model [22,25] is built on the basis of LWFs generated from density functional theory (DFT) calculations. The screened Coulomb interactions between LWFs are computed in the constrained random-phase approximation

*Authors to whom correspondence should be addressed: xifanwu@temple.edu and xiaoshan.xu@unl.edu

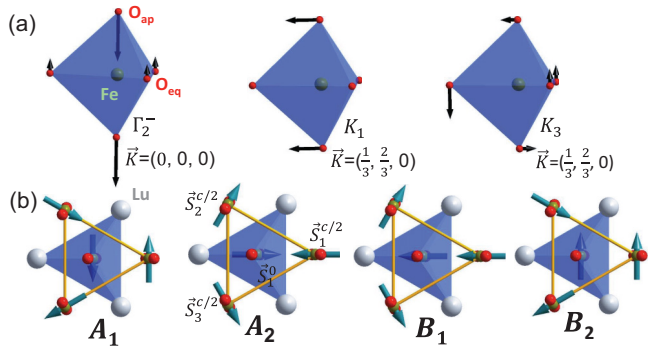

FIG. 1. (Color online) (a) Displacement patterns of the FeO_5 local environment (trigonal bipyramid) in the three phonon modes that freeze in the $P6_3/mmc \rightarrow P6_3cm$ structural transition in hexagonal ferrites (h-$RFeO_3$). The arrows indicate the relative displacement of the atoms. $\vec{K}$ is the wave vector of the modes in the reciprocal space of the $P6_3/mmc$ structure. (b) Four independent spin structures (A_1, A_2, B_1, and B_2) of the 120-degree magnetic orders viewed along the c axis. The arrows indicate the spins ($\vec{S}_i^{Z_{Fe}}$) on the Fe sites. The Fe sites shown in the polyhedra are in the $Z_{Fe} = 0$ layer while all the other Fe sites are in the $Z_{Fe} = c/2$ layers. In the B (A) phase, $\vec{S}_1^0$ is parallel (antiparallel) to $\vec{S}_1^{c/2}$.

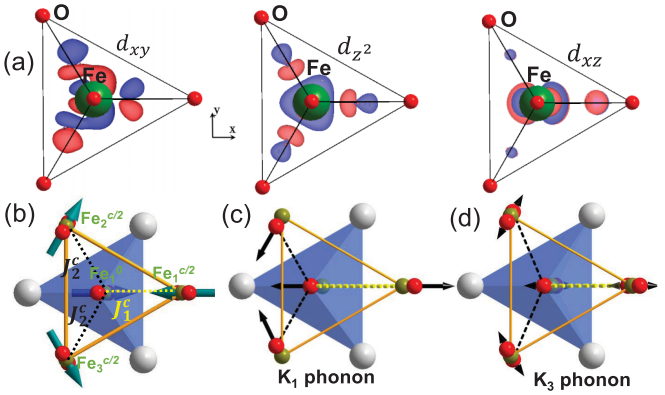

FIG. 2. (Color online) (a) Representative d_{xy}, d_{z^2}, and d_{xz}-like LWFs viewed from [001] direction. (b) Illustrations of two independent SSE paths J_1^c and J_2^c between Fe_0 at $z/c = 0$ and three neighboring iron ions Fe_1, Fe_2, and Fe_3 at $z/c = 1/2$ (c) Atomic displacements of the K_1 phonon mode. (d) Atomic displacements of the K_3 phonon mode, viewed from [001] direction.

[25–27]. The calculations of spin phonon coupling is performed within DFT+U scheme [25,28]. We have adopted the four-state method [29] in computing the exchange coupling strengths. hLFO films (50 nm thick) were grown on Al_2O_3 (0001) substrates with and without a (30 nm) Pt buffer layer using pulsed laser deposition. The x-ray diffraction (XRD) and x-ray absorption spectroscopy (XAS) measurements were carried out in the 6-ID-B beam line on the h-$LuFeO_3/Al_2O_3$ film and in the 4-ID-C beam line on the h-$LuFeO_3$/Pt/Al_2O_3 film at the Advanced Photon Source at various temperature.

III. RESULTS AND DISCUSSION

In hexagonal ferrites, the exchange interaction between the Fe sites can be written as

$$H_{ex} = H_{ex}^{a-b} + H_{ex}^{c} \tag{1}$$

where H_{ex}^{a-b} is the intralayer exchange interaction and H_{ex}^{c} is the interlayer exchange interaction considering only the nearest neighbors.

As shown in Fig. 2, the intralayer SE interaction $H_{ex}^{a-b} = \sum_{i,j,Z_{Fe}} \mathcal{J}_{i,j}^{a-b} \vec{S}_i^{Z_{Fe}} \cdot \vec{S}_j^{Z_{Fe}}$ between two nearest neighbor (NN) Fe atoms at site i and j are mediated by corner sharing oxygen atoms. In order to elucidate the electronic structural origin, we employ the extended KK model, and the SE coupling can be expressed as

$$\mathcal{J}_{i,j}^{a-b} = \sum_{\alpha,\alpha'} J_{\alpha,\alpha'}^{\mathrm{AFM}} + \sum_{\alpha,\beta} J_{\alpha,\beta}^{\mathrm{FM}}. \tag{2}$$

The first term in Eq. (2) describes the AFM-type coupling resulting from virtual hopping processes between two half-filled d bands; while the second term depicts the competing FM-type coupling from hoppings from a half-filled d orbital (α) to empty ones (β) [25]. The computed individual exchange interaction as well as the overall SE coupling J_{MOD}^{a-b} for both hLFO and hLMO are presented in Table I. The total exchange couplings J_{DFT}^{a-b} from the direct fit of the total DFT energies are also shown.

According to the local environment (Fig. 1), the 3d orbitals in Fe and Mn are split into $e''(xz,yz)$, $e'(x^2-y^2,xy)$, and $a_1'(z^2)$ levels by the crystal field, with increasing energy respectively [30,31]. It can be seen that the largest SE interactions are contributed by the diagonal hopping processes involving d orbitals of e' symmetry. This is consistent with the physical expectation that SE is of intralayer nature while d_{xy} and $d_{x^2-y^2}$ are the only d orbitals lying mostly inside the ab plane. Centered on the magnetic ions, these d-like LWFs are also connected with the first neighboring magnetic atoms through hybridization with the shared oxygen atoms on the bipyramids. As a result, a strong oxygen p character is found on the lobe of the LWFs, pointing to each of the three neighboring oxygen atoms. Considering such d-like LWFs on the hexagonal lattices, a large AFM hopping integral is thus expected along the path of Fe(Mn)-O-Fe(Mn) [32]. Based on the same orbital symmetry argument, it can be easily seen that the diagonal hopping is relatively smaller for $a_1'(z^2)$ character and almost zero for e'' character. This is because d_{z^2} and d_{xz}

TABLE I. Individual and total intralayer exchange interaction (meV) in both hLFO and hLMO [25].

$J_{\alpha,\alpha'(\beta)}$		d_{xy}	$d_{x^2-y^2}$	d_{z^2}	d_{xz}	d_{yz}	J_{MOD}^{ab}	J_{DFT}^{ab}
hLFO	d_{xy}	9.49	3.65	3.20	1.14	0.47	45.2	49.7
	$d_{x^2-y^2}$	0.68	9.90	0.88	1.04	0.05		
	d_{z^2}	1.25	5.05	3.58	1.25	0.27		
	d_{xz}	0.56	0.09	0.14	0.01	0.06		
	d_{yz}	0.32	1.00	0.65	0.37	0.06		
hLMO	d_{xy}	10.15	5.81	−0.64	1.17	0.78	29.3	30.7
	$d_{x^2-y^2}$	1.28	10.9	−2.71	0.85	0.12		
	d_{z^2}							
	d_{xz}	0.41	0.17	−0.43	0.01	0.08		
	d_{yz}	0.39	0.85	−0.19	0.31	0.04		

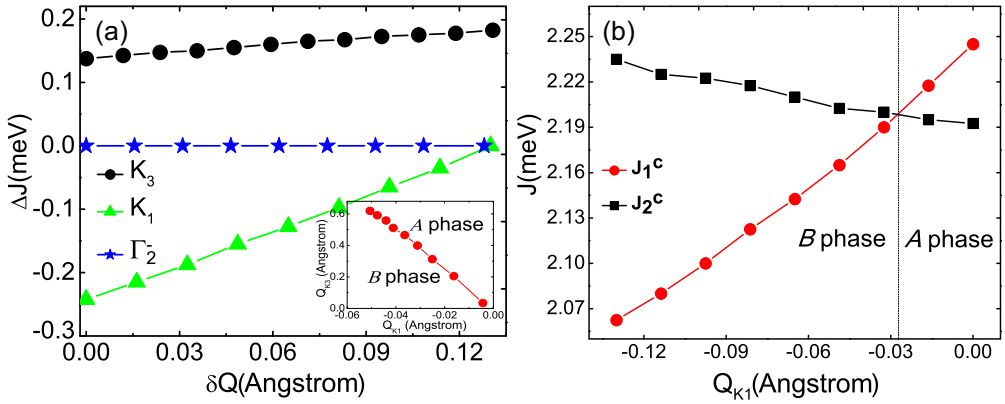

FIG. 3. (Color online) (a) $\Delta J(\delta Q) = J(Q) - J(Q_0)$ for each individual K_1, K_3, and Γ_2^- phonon mode, where $\delta Q = Q - Q_0$ and Q_0 is the value at 300 K, while the other two phonon displacements are kept as zero. Inset: theoretical phase diagram as functions of mode amplitudes of K_1 and K_3. (b) J_1^c and J_2^c as functions of Q_{K_1}, while Q_{K_3} and $Q_{\Gamma_2^-}$ are fixed at the experimental values [25].

(d_{yz}) require that the main orbital lobe be located along z or within the xz (yz) plane, which makes the hopping integrals much smaller.

Strikingly, the SE interactions also show fundamental differences between the two materials. In hLFO (Fe^{3+}:$3d^5 4s^0$), the d_{z^2} orbital of a_1' symmetry is singly occupied, and SE interactions can only be of AFM types. However, d_{z^2} is empty in hLMO (Mn^{3+}:$3d^4 4s^0$), SE interactions are thus composed of competing AFM and FM types, and the coupling strength is further reduced by the forbidden hopping involving the empty d_{z^2}. Thus, a significantly larger AFM coupling energy is observed in hLFO. This is consistent with the higher Neél temperature in hLFO observed in experiment in addition to the larger spin on the Fe site.

Having established the electronic origin of the large intralayer exchange coupling, we now focus on the interlayer exchange coupling $H_{ex}^c = \sum_{i,j,Z_{Fe}} \mathcal{J}_{i,j}^c \vec{S}_i^{Z_{Fe}} \cdot \vec{S}_j^{Z_{Fe}+\frac{c}{2}}$ in hLFO. This is the key to understanding the mechanism of SR and weak FM moment below T_R [5]. In contrast to the SE nature of intralayer exchange, the interlayer Fe ions are coupled by the super-super-exchange (SSE) interaction [33], in which one Fe atom at $Z_{Fe} = 0$ is in exchange interaction with three first neighbor Fe atoms at $Z_{Fe} = c/2$ mediated by two apical oxygen atoms (O_{ap}). Due to the $P6_3cm$ structure in Fig. 3 (b), the three SSE paths can be further simplified by two independent SSE coupling strengths: J_1^c through Fe_1^0-O- $\cdots$ -O-$Fe_1^{\frac{c}{2}}$ and J_2^c through Fe_1^0-O- $\cdots$ -O-$Fe_2^{\frac{c}{2}}$. As a result, the H_{ex}^c spin Hamiltonian in Eq. (1) can be rewritten as $H_{ex}^c = \sum_{i,Z_{Fe}} (J_1{}^c - J_2{}^c) \vec{S}_i^{Z_{Fe}} \cdot \vec{S}_i^{Z_{Fe}+\frac{c}{2}}$. Obviously, the sign of $\Delta J = J_1^c - J_2^c$ determines the preferred alignment between $\vec{S}_i^{Z_{Fe}}$ and $\vec{S}_i^{Z_{Fe}+\frac{c}{2}}$: parallel ($B$ phase) if $\Delta J < 0$; antiparallel (A phase) if $\Delta J > 0$; no alignment if $\Delta J = 0$, which is the case for $P6_3/mmc$ structure.

Since the nonzero ΔJ comes from the structural distortion ($P6_3/mmc \rightarrow P6_3cm$), the low temperature spin reorientation must have a structural origin. Here we investigate the dependence of ΔJ on the three phonon modes K_1, K_3, and Γ_2^- that are responsible for the structural distortion [25]. We use DFT to calculate the ΔJ as functions of phonon mode displacements (Q_p, where $p = K_1, K_3$, and Γ_2^-) and the results are shown in Fig. 3(a). It can be seen that ΔJ depends on the displacement of each phonon mode rather differently.

Clearly, the K_1 phonon mode has the largest effect on SR. This can be identified by the steepest slope of ΔJ when K_1 is increased perturbatively, yielding a linear coefficient $\frac{\delta \Delta J}{\delta Q_{K_1}} \sim 1.9$ meV/Å. This suggests a strong tendency of K_1 in driving hLFO from B phase ($\Delta J < 0$) into A phase ($\Delta J > 0$). Indeed this is also consistent with the physical expectation of atomic displacements under the K_1 mode. The K_1 phonon is a Brillouin zone (BZ) boundary mode and is of pure in-plane nature. The atomic displacements of the K_1 phonon mostly involve the O_{ap} of FeO_5 (Fig. 1). As shown in Fig. 2(c), the effects of the K_1 are as follows: O_{ap} of Fe_1^0 moves away from that of $Fe_1^{\frac{c}{2}}$, causing J_1^c to decrease; and O_{ap} of Fe_1^0 moves closer to that of $Fe_2^{\frac{c}{2}}$ and $Fe_3^{\frac{c}{2}}$, causing J_2^c to increase. As a result, K_1 is strongly coupled to the ΔJ.

The K_3 phonon mode can be described by the rotation of FeO_5 [Fig. 1(a)] also located at BZ boundary. The atomic displacements of the K_3 mode include all the O_{ap} of the FeO_5. However, due to its rotational nature, the atomic displacement of the O_{ap} alternate their directions along c as shown in Fig. 2(d). As a result, the overall lengths of J_1^c and J_2^c paths are barely changed except that the Fe atom is slightly moved away from its equilibrium positions in $P6_3/mmc$ symmetry. Compared with the direct tunability of ΔJ by the K_1 mode, the K_3 phonon is expected to be a second-order effect in SR. Indeed, our DFT calculation predicts a much weaker variation of ΔJ with increased K_3 phonon mode amplitude, in which the linear coefficient $\frac{\delta \Delta J}{\delta Q_{K_3}} \sim 0.3$ meV/Å is about one order of magnitude smaller than that of K_1. Similar to that of K_1 mode, the slope is also positive, favoring the SR from B to A phase.

Finally, we focus on the coupling between Γ_2^- and ΔJ. Γ_2^- is the ferroelectric phonon mode at zone center. The atomic displacements of this mode involve all the Lu, O, and Fe atoms moving along c. However, the displacements of the two O_{ap} of one bipyramid are exactly the same. As a result, the SSE paths in J_1^c and J_2^c are changed uniformly. Not surprisingly, our theory predicts a zero dependence of ΔJ on Γ_2^- mode amplitude. It indicates that this ferroelectric distortion alone does not play any role in SR.

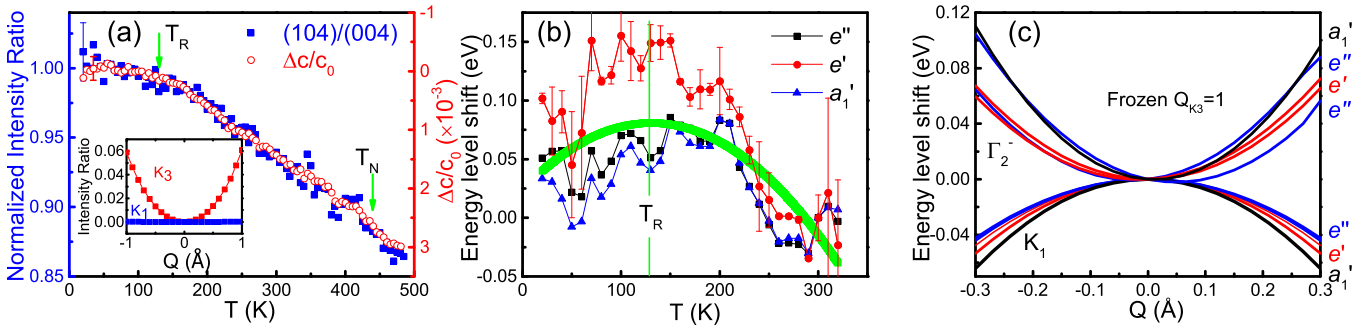

FIG. 4. (Color online) Structural changes indicated by the XRD and XAS. (a) The XRD intensity ratio between the (104) and (004) peaks (normalized to the 30 K value) and the change of lattice constant c (with respect to the 30 K value) as functions of the temperature (the representative error bars are shown). Inset: the simulated intensity ratio between the (104) and (004) peaks as functions of phonon displacements. (b) The change of Fe-3d crystal field levels (relative to the 300 K values) as functions of the temperature (the error bars for e' levels are shown as examples); the bold line is a guide to the eye to highlight the common peak-like feature. (c) Simulated change of Fe-3d levels as functions of phonon displacements [25].

The significantly different coupling strengths of ΔJ with the phonon modes suggests the primary role of the K_1 phonon mode in SR of hLFO. Indeed, when the K_1 mode is frozen into the experimental structural coordinates at $T = 300$ K perturbatively, J_1^c and J_2^c rapidly increase and decrease respectively, and SR occurs at the crossing point as shown in Fig. 3(b) separating the B from A phases. Below, we show that Q_{K_3} saturates close to T_R, while Q_{K_1} changes significantly from 300 to 20 K using XRD and XAS measurements.

As shown in Fig. 4(a), the temperature dependence of the normalized intensity ratio between (104) and (004) peaks appears to saturate when temperature is lowered to T_R. We attribute the saturation to the slow variation of the K_3 phonon at low temperature, because K_3 is expected to have a dominant effect here, according to the simulated intensity ratio [Fig. 4(a) inset] [34], while the zone center mode Γ_2 is expected to have no effect. The saturation of the K_3 mode can be further confirmed by the temperature dependence of the lattice constant c which follows closely that of the intensity ratio, as shown in Fig. 4(a). The displacement of the K_3 mode includes a rotation of the FeO_5 trigonal bipyramid, which changes the shape of the unit cell by enlarging a and reducing c [7]; the change of c (Δc) is proportional to ΔQ_{K_3} for small change of Q_{K_3}. The matching temperature dependence in Fig. 4(a) suggests that the change of c is indeed caused by the K_3 mode which saturates at low temperature.

XAS measurements suggest that the K_1 mode undergoes a gradual change at low temperature. Previously, we assigned the Fe-3d crystal levels using the XAS at room temperature [25,30]. As shown in Fig. 4(b), the temperature dependences of the energy levels all show broad peak-like features with the maxima close to T_R. The crystal field levels of Fe-3d are expected to be sensitive to the shape of FeO_5. As shown in Fig. 1(a), the K_3 mode causes a rotation of the FeO_5 while the K_1 or Γ_2^- modes cause distortions of the FeO_5, so the energy-level shifts observed in Fig. 4(c) are most likely generated by the change of Q_{K_1} or $Q_{\Gamma_2^-}$. Figure 4(c) shows a simulation [25] of the energy-level change of the crystal field levels as functions of Q_{K_1} or $Q_{\Gamma_2^-}$ with respect to the value when all the mode displacements are zero. According to the simulation, the K_1 mode generates a maximum at $Q_{K_1} = 0$ while $Q_{\Gamma_2^-}$ generates a minimum at $Q_{\Gamma_2^-} = 0$; this is because the K_1 mode moves both O_{ap} atoms away from the Fe sites and makes the FeO_5 larger while the Γ_2^- mode pushes one O_{ap} atom close to the Fe site. Comparing the simulation and the observation, we infer that the K_1 mode changes gradually when the temperature is lowered, in order to generate the maximum [25]; this is consistent with the theoretical prediction in which Q_{K_1} changes when the temperature is lowered and causes the transition from antiferromagnetism in the B_2 phase to weak ferromagnetism in the A_2 phase.

IV. CONCLUSION

The roles of all three structural distortions are elucidated in hLFO: the instability of the K_3 mode is the driving force of the $P6_3/mmc \rightarrow P6_3cm$ structural transition; the improper ferroelectricity of the Γ_2^- mode is induced by the frozen K_3 mode [13,15]; and the competing effect between K_1 and K_3 modes determines the magnetic ordering and drives the magnetic phase transition. If the K_1 mode can be tuned by interface engineering [35–37], the T_R can be increased, achieving the spontaneous electric and magnetic polarizations and their couplings at room temperature.

ACKNOWLEDGMENTS

This work is supported by Air Force Office of Scientific Research under Grant No. FA9550-13-1-0124 (X.W.). Computational support is provided by the National Energy Research Scientific Computing Center and by the National Science Foundation through XSEDE resources provided by the XSEDE Science Gateways program (Award No. TG-DMR120045). Research was supported by the US Department of Energy, Basic Energy Sciences, Materials Sciences and Engineering Division (T.Z.W. and X.S.X.). We also acknowledge partial funding support from the National Basic Research Program of China (973 Program) under Grant No. 2011CB921801 (J.S.), from the National Natural Science Funds of China, Grant No. 11374275 (L.H.) and from the US DOE Office of

Basic Energy Sciences, Grant No. DE-SC0002136 (W.B.W.). Use of the Advanced Photon Source was supported by the US Department of Energy, Office of Science, Office of Basic Energy Sciences, under Contract No. DE-AC02-06CH11357. X.M.C. acknowledges support from the National Science Foundation under Grant No. 1053854. X.W. is grateful for useful discussions with Andrei Malashevich, Craig Fennie, Weida Wu, and David Vanderbilt.

[1] M. Stengel, N. A. Spaldin, and D. Vanderbilt, Nat. Phys. **5**, 304 (2009).
[2] H. Fu and R. E. Cohen, Nature (London) **403**, 281 (2000).
[3] S. Lee, A. Pirogov, M. Kang, K.-H. Jang, M. Yonemura, T. Kamiyama, S.-W. Cheong, F. Gozzo, N. Shin, H. Kimura, Y. Noda, and J.-G. Park, Nature (London) **451**, 805 (2008).
[4] J. H. Lee *et al.*, Nature (London) **466**, 954 (2010).
[5] W. Wang, J. Zhao, W. Wang, Z. Gai, N. Balke, M. Chi, H. N. Lee, W. Tian, L. Zhu, X. Cheng, D. J. Keavney, J. Yi, T. Z. Ward, P. C. Snijders, H. M. Christen, W. Wu, J. Shen, and X. Xu, Phys. Rev. Lett. **110**, 237601 (2013).
[6] E. Magome, C. Moriyoshi1, Y. Kuroiwa1, A. Masuno and H. Inoue, Jpn. J. Appl. Phys. **49**, 09ME06 (2010).
[7] A. Muñoz, J. A. Alonso, M. J. Martínez-Lope, M. T. Casáis, J. L. Martínez, and M. T. Fernández-Díaz, Phys. Rev. B **62**, 9498 (2000).
[8] A. R. Akbashev, A. S. Semisalova, N. S. Perov, and A. R. Kaul, Appl. Phys. Lett. **99**, 122502 (2011).
[9] I. Dzyaloshinsky, J. Phys. Chem. Solids **4**, 241 (1958).
[10] T. Moriya, Phys. Rev. **120**, 91 (1960).
[11] A. Malashevich and D. Vanderbilt, Phys. Rev. Lett. **101**, 037210 (2008).
[12] J. Hong, A. Stroppa, J. Íñiguez, S. Picozzi, and D. Vanderbilt, Phys. Rev. B **85**, 054417 (2012).
[13] H. Das, A. L. Wysocki, Y. Geng, W. Wu, and Craig J. Fennie, Nat. Commun. **5**, 2998 (2014).
[14] Y. Geng, H. Das, A. L. Wysocki, X. Wang, S.-W. Cheong, M. Mostovoy, C. J. Fennie, and W. Wu, Nat. Mater. **13**, 163 (2014).
[15] C. J. Fennie and K. M. Rabe, Phys. Rev. B **72**, 100103(R) (2005).
[16] N. A. Spaldin, S.-W. Cheong, and R. Ramesh, Phys. Today **63**, 38 (2010).
[17] J. Wang *et al.*, Science **299**, 1719 (2003).
[18] J. B. Neaton, C. Ederer, U. V. Waghmare, N. A. Spaldin, and K. M. Rabe, Phys. Rev. B **71**, 014113 (2005).
[19] T. Lancaster, S. J. Blundell, D. Andreica, M. Janoschek, B. Roessli, S. N. Gvasaliya, K. Conder, E. Pomjakushina, M. L. Brooks, P. J. Baker, D. Prabhakaran, W. Hayes, and F. L. Pratt, Phys. Rev. Lett. **98**, 197203 (2007).
[20] X. Fabrèges, S. Petit, I. Mirebeau, S. Pailhès, L. Pinsard, A. Forget, M. T. Fernandez-Diaz, and F. Porcher, Phys. Rev. Lett. **103**, 067204 (2009).
[21] P. J. Brown and T. Chatterji, J. Phys. Condens. Matter **18**, 10085 (2006).
[22] K. I. Kugel and D. I. Khomskii, Sov. Phys. Usp. **25**, 231 (1982).
[23] N. Marzari, A. A. Mostofi, J. R. Yates, I. Souza, D. Vanderbilt *et al.*, Rev. Mod. Phys. **84**, 1419 (2012).
[24] P. H.-L. Sit, Roberto Car, Morrel H. Cohen, and A. Selloni, Inorg. Chem. **50**, 10259 (2011).
[25] See Supplemental Material at http://link.aps.org/supplemental/10.1103/PhysRevB.90.014436 for more detailed information on the theoretical model and calculation, phonon mode decomposition, analysis of the x-ray absorption spectra, and simulation of crystal field levels.
[26] I. V. Solovyev, M. V. Valentyuk, and V. V. Mazurenko, Phys. Rev. B **86**, 054407 (2012).
[27] I. V. Solovyev, J. Phys: Condens. Matter **20**, 293201 (2008).
[28] G. Kresse and J. Furthmüller, Phys. Rev. B **54**, 11169 (1996).
[29] H. J. Xiang, E. J. Kan, S.-H. Wei, M.-H. Whangbo, and X. G. Gong, Phys. Rev. B **84**, 224429 (2011).
[30] W. Wang, H. Wang, X. Xu, L. Zhu, L. He, E. Wills, X. Cheng, D. J. Keavney, J. Shen, X. Wu, and X. Xu, Appl. Phys. Lett. **101**, 241907 (2012).
[31] D.-Y. Cho, J.-Y. Kim, B.-G. Park, K.-J. Rho, J.-H. Park, H.-J. Noh, B. J. Kim, S.-J. Oh, H.-M. Park, J.-S. Ahn, H. Ishibashi, S.-W. Cheong, J. H. Lee, P. Murugavel, T. W. Noh, A. Tanaka, and T. Jo, Phys. Rev. Lett. **98**, 217601 (2007).
[32] P. W. Anderson, Phys. Rev. **79**, 350 (1950).
[33] M.-H. Whangbo, H.-J. Koo, and D. Dai, J. Solid. State. Chem. **176**, 417 (2003).
[34] B. D. Cullity, *Elements of X-Ray Diffraction* (Addison-Wesley, Reading, MA, 1956).
[35] J. H. Lee and K. M. Rabe, Phys. Rev. Lett. **104**, 207204 (2010).
[36] O. Diéguez, K.M. Rabe, and D. Vanderbilt, Phys. Rev. B **72**, 144101 (2005).
[37] J. Junquera and P. Ghosez, Nature (London) **422**, 506 (2003).